



## Effective demineralization of malachite green, and Janus green blue dyes with nickel oxide nanoparticles: a novel green chemistry method

N. Saikumari, Raja Venkatesan, Suseela Jayalakshmi, Maher M. Alrashed & Seong-Cheol Kim

To cite this article: N. Saikumari, Raja Venkatesan, Suseela Jayalakshmi, Maher M. Alrashed & Seong-Cheol Kim (30 Jul 2025): Effective demineralization of malachite green, and Janus green blue dyes with nickel oxide nanoparticles: a novel green chemistry method, International Journal of Phytoremediation, DOI: [10.1080/15226514.2025.2538644](https://doi.org/10.1080/15226514.2025.2538644)

To link to this article: <https://doi.org/10.1080/15226514.2025.2538644>



© 2025 Taylor & Francis Group, LLC



Published online: 30 Jul 2025.



Submit your article to this journal [↗](#)



Article views: 272




View related articles [↗](#)



View Crossmark data [↗](#)



# Effective demineralization of malachite green, and Janus green blue dyes with nickel oxide nanoparticles: a novel green chemistry method

N. Saikumari<sup>a</sup>, Raja Venkatesan<sup>b,c</sup> , Suseela Jayalakshmi<sup>d</sup>, Maher M. Alrashed<sup>e</sup>, and Seong-Cheol Kim<sup>b</sup>

<sup>a</sup>Department of Science and Humanities, R.M.K. College of Engineering and Technology, Chennai, India; <sup>b</sup>School of Chemical Engineering, Yeungnam University, Gyeongsan, Republic of Korea; <sup>c</sup>Department of Biomaterials, Saveetha Dental College and Hospitals, SIMATS, Saveetha University, Chennai, India; <sup>d</sup>Department of Chemistry, School of Basic Sciences, VISTAS, Chennai, India; <sup>e</sup>Chemical Engineering Department, College of Engineering, King Saud University, Riyadh, Saudi Arabia

## ABSTRACT

Solution combustion method (SCM), with urea as a fuel, is a convenient method to synthesize nickel oxide (NiO) nanoparticles. NiO nanoparticles have been characterized using UV-visible spectroscopy (UV-Vis), X-ray diffraction (XRD), scanning electron microscopy (SEM) with EDX, transmission electron microscopy (TEM), and BET surface area determination. The average size of the NiO nanoparticles is 22 nm, and it has a band gap of 3.17 eV. It also showed a cubical assembly. Furthermore, the average size of NiO nanoparticles has been confirmed *via* TEM analysis, which is 25 nm. Malachite green (MG) and Janus green blue (JGB) dye degradation under solar irradiation could be prevented with synthetic NiO nanoparticles with the modification of catalytic concentration, pH, and the dye concentrations. The NiO nanoparticles demonstrated superior photocatalytic degradation against MG, and JGB as 97% and 96%. The catalyst concentration, pH, and dye concentration were varied with the aim to measure the degradation efficiency. A dye concentration of  $1 \times 10^{-4}$  mol/dm<sup>3</sup> and a dye pH of 4 provided the most effective results.

## NOVELTY STATEMENT

The novelty of this work lies in the integration of green chemistry with the NiO nanoparticles, which are prepared *via* a solution combustion method (SCM) utilizing urea as a fuel. As a nano-catalyst, NiO nanoparticles offer a nontoxic, cost-effective, and highly efficient alternative for the photocatalytic degradation of these dyes. The study systematically identifies the optimal operational parameters for dye degradation, including a dye concentration of  $1 \times 10^{-4}$  mol/dm<sup>3</sup> and a pH of 4, while underscoring the environmentally benign synthesis of NiO nanoparticles.

## KEYWORDS

NiO nanoparticles; photo catalysis; photo catalytic degradation; spectral analysis

## 1. Introduction

Wastewater containing dye has harmful effects on aquatic life and poses major issues for neighboring water frames and soil organic matter (Saikumari *et al.* 2019; Lin *et al.* 2025). Innovative new techniques to secure safely available water from household, farming, and other sources of activity has become necessary due to the depletion of water reserves and over exploitation of water resources that already exist. The natural environment is at risk by the 25%–30% hazardous dyes discovered in wastewater from industries as pulp and paper, paints & varnishes, textiles, cosmetics, ink, and plastics. As a result, scientists have dedicated considerable attention to developing methods for treating wastewater contaminated with these organic dyes. One of the biggest problems in the industries is color removal (Balarak *et al.* 2020). In addition to their inability to totally eradicate color, conventional treatment techniques have the potential to spread contaminants from one medium to another, being done with newer techniques. Photo catalysis has been

demonstrated to be an effective, appropriate, and potentially beneficial method for reducing organic pollutants, particularly dyes, in industrial wastewaters (Ahamed *et al.* 2019; Bomila *et al.* 2019; Balarak *et al.* 2021). Because of their structural and functional characteristics, semiconductor photo catalysis stands out among the others as a promising technique.

Heterogeneous photocatalysis has been demonstrated to be an effective, appropriate, and potentially beneficial method for reducing organic pollutants, particularly dyes, in industrial wastewaters (Al-Musawi *et al.* 2021; Jiang *et al.* 2025). It is a useful mechanism for treating wastewater containing dyes because it transforms hazardous, poisonous contaminants into safe byproducts without endangering the environment (Balarak, Al Musawi, *et al.* 2020; Balarak, Zafariyan, *et al.* 2020). As photo catalysts, a variety of metal oxide semiconductors, like nickel (Saffarzadeh *et al.* 2019), titanium (Balarak *et al.* 2021), zinc, copper, tin, zirconium, tungsten, and carbon nanotubes, as well as mixed compounds of bismuth,

silver are used in dye degradation, and heterotrophic denitrification (Zhu *et al.* 2023; Fardood, Ganjkanlu, *et al.* 2024; Fardood, Moradnia, and Aminabhavi 2024; Fardood, Moradnia, Zare *et al.* 2024; Fardood, Moradnia, Ganjkanlu, *et al.* 2024). In a variety of fields, like photovoltaic devices, optoelectronics, photoelectric, drug delivery, capacitors, hydrogen storage, gas sensors, catalysts, battery, and hybrid capacitors, NiO nanoparticles have displayed use in everyday life. Its electrical conductivity, chemical stability, mechanical, thermal and magnetic characteristics make NiO nanoparticles a popular choice among these applications (Taghizadeh *et al.* 2018; Ebin 2018).

Nickel oxide nanoparticle can take various forms as particles, tubes, rods, spheres, belts, prism, ribbons, rings, sheets, and flakes in nano size during the synthesis (Faraji *et al.* 2023; Fardood, Ganjkanlu, *et al.* 2024; Fardood, Moradnia, and Aminabhavi 2024; Fardood, Moradnia, Zare *et al.* 2024; Fardood, Moradnia, Ganjkanlu, *et al.* 2024). Trypan blue organic dye was degraded by Faraji *et al.* (2023) to show how NiO nanoparticles could be prepared in an economical and environmentally responsible manner. The methods that can be used to create these nanoparticles include electrochemical, sol-gel, electro-deposition, thermo-chemical processing (Mansour and Mir 2017; Abd-El-Lateef *et al.* 2020; Ahmad *et al.* 2022; Jamil *et al.* 2022; Sivagami and Asharani 2022; Hassan *et al.* 2023; Salim and Tarabiah 2023; Fardood *et al.* 2024), solution combustion, and ultrasound-assisted leaching (Rao *et al.* 2024). The SCM is thought to be normal, easy and quicker than other approaches and is considered for the synthesis as well as for further studies. Because of the unique characteristics with respect to crystallite size, surface area and quantization effect etc. (Jamal *et al.* 2011; Chaudhary *et al.* 2013; Yadav *et al.* 2014).

In this work the sample pollutants were common textile dyes namely Malachite green and Janus green. Malachite green is a problematic antibacterial agent used in aquaculture as well as a dye. Paper, leather, and silk are also dyed with a similar material. Cell biology and tissues are investigated with the microscope using it as a biological stain. MG is a harmful pollutant released from industries and lethal due to its potential carcinogenicity, mutagenicity, and teratogenicity. Similarly, Janus Green B is another basic dye and is used to stain mitochondria. These dyes generally irritate the eyes, affect respiratory system and

also toxic to living organisms. Long exposure to these dyes may cause dermatitis, conjunctivitis and infect throat, nose, lungs etc. The preparation and characteristic analysis of NiO nanoparticles as well as the degradation of MG and JGB dyes in the presence of sunlight were considered to be the main objectives of this study. The experimental setup focuses on efficient degradation under mild conditions, making the process more accessible for practical implementation.

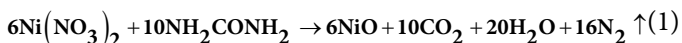
## 2. Materials and methods

### 2.1. Materials

We received the chemicals from Sigma-Aldrich, such as and nickel nitrate  $\text{Ni}(\text{NO}_3)_2 \cdot 6\text{H}_2\text{O}$  (99% pure). The dyes, Malachite green (MG) ( $\lambda_{\text{max}}$  617 nm), and Janus green blue (JGB) ( $\lambda_{\text{max}}$  492 nm) were obtained from Sigma-Aldrich. The chemical structures of methylene blue and malachite green are shown in Figure 1. Acetone (98% pure), urea ( $(\text{NH}_2\text{CONH}_2)$ , 98% pure), and double-distilled water were purchased from Merck. The materials were used as such given.

### 2.2. Synthesis of nickel oxide nanoparticles

Exploiting urea as a fuel and commercial nickel nitrate, the solution combustion method (SCM) is utilized to synthesize NiO nanoparticles. A deionized water has been to employed to dissolve nickel nitrate (10.96 g) and urea (6 g) to determine their stoichiometric composition. In addition, the solution was burned in a muffle furnace that had been warmed to 600°C. The resulting particles were employed for characterization and photocatalytic activity after being cooled and finely milled. The resulting particles were employed in characterization and degrading processes. The possible chemistry reaction is given below.



As synthesized catalysts were characterized by different physio-chemical analytical methods and also the salient features of the equipment's are described.

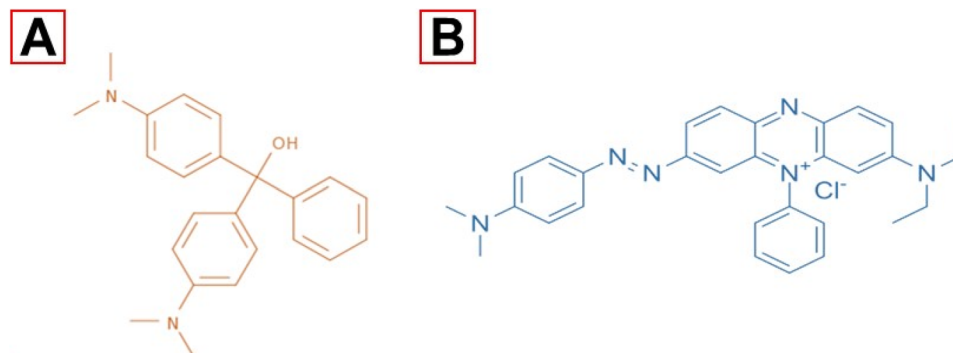


Figure 1. Chemical structures of (A) malachite green (MG), and (B) janus green blue (JGB).

## 2.3. Characterization

The NiO nanoparticles were characterized using XRD (6000, Shimadzu Scientific) for the determination of their mineralogical phase and crystalline structures. The SEM and TEM techniques made by Zeiss Auriga were explored to determine their morphologies, while the EDX was used to determine their elemental compositions. The SAED analysis also assisted to determine the crystallinity of the nanocomposites. The surface properties and functional groups present on the nanomaterials were investigated using BET (NOVA4200e, Quantachrome UK). Also, the pH point of zero charges (pHpzc) was carried out on the nano adsorbents of  $\text{ZnWO}_4$  and  $\text{ZnWO}_4\text{@BCN/C}$  using the salt addition method. Briefly, 30 mL of 0.02 M NaCl solution was added to different beakers, thereafter adjusting the pH values to 2, 4, 6, 8, 10, and 12 using 0.02 M HCl and 0.02 M NaOH. 0.20 g of the nano adsorbents was added to each beaker and stirred using a magnetic stirrer at 250 rpm for 5 h. The solutions were allowed to settle and the final pH values were determined using a pH meter.

## 3. Result and discussion

### 3.1. UV-visible absorption spectroscopy

NiO nanoparticles may effectively absorb UV light due to their bandgap. Tauc's plot was used to calculate the bandgap. As indicated in Figure 2A, the bandgap for the NiO nanoparticles was calculated by extrapolating the curve from the plot of  $(\alpha h\nu)^2$  against  $(\alpha h\nu)^2$ . There, the coefficient of optical absorption is denoted by  $\alpha$ , whereas the frequency is indicated by  $\nu$ . The resulted in NiO NPs' absorption spectra can be seen by the extrapolated bandgap energy, which is calculated to be 3.17 eV. According to the Tauc relation, which was presented by El-Kemary *et al.*, Puttaswamy *et al.* (2018), Kumar *et al.* (2019), and El-Latheef *et al.*, the band gap energy of NiO nanoparticles has been calculated to be 3.17 eV.

### 3.2. XRD analysis

Figure 2B represents the XRD pattern of the NiO nanoparticles. The diffraction peak was distinct and crystalline. 111,

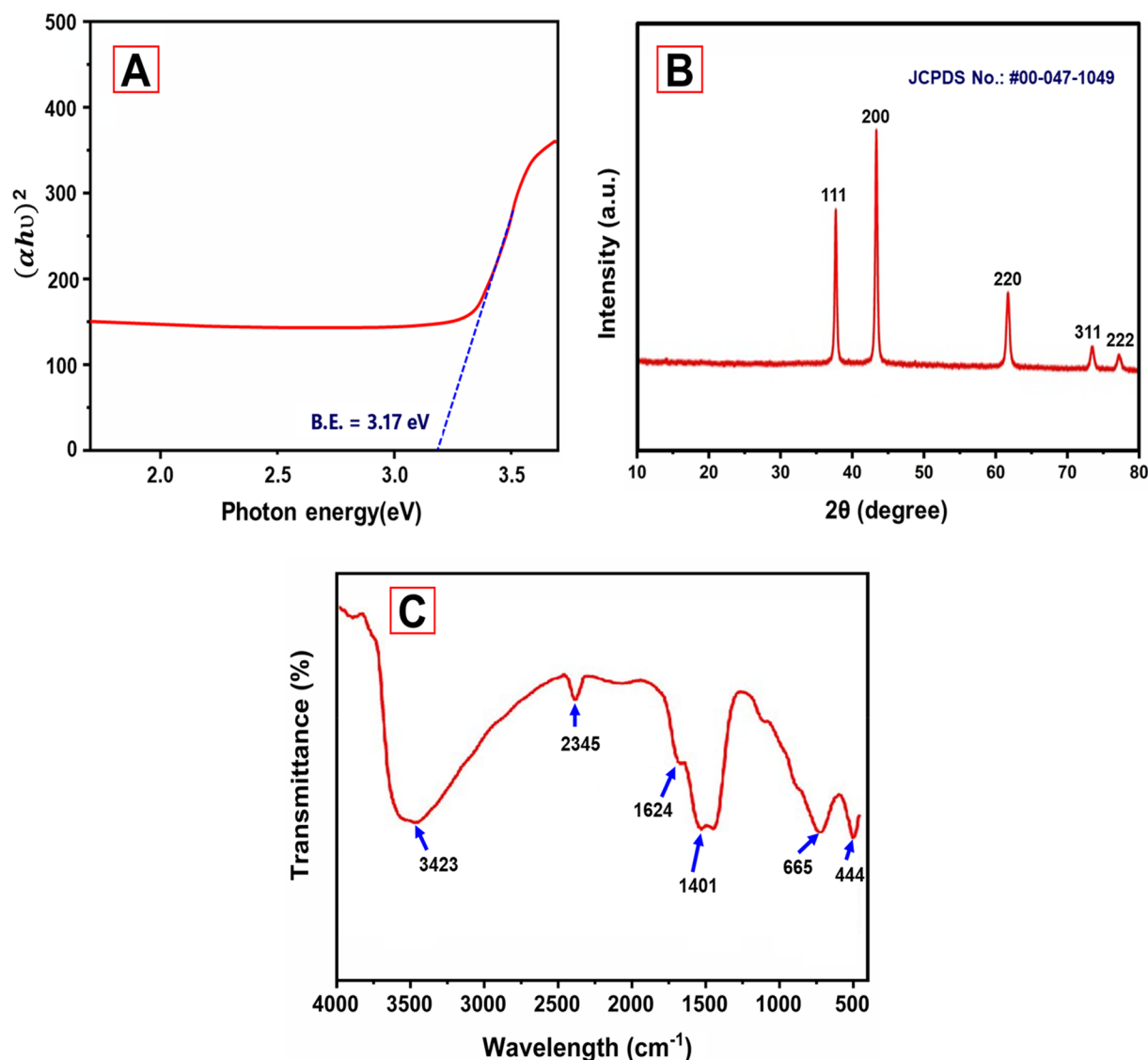


Figure 2. (A) Tauc plot, (B) XRD pattern, and (C) FTIR spectra of the synthesized NiO nanoparticles.

200, 220, 311, and 222 planes of NiO nanoparticles are denoted by the diffraction peaks  $2\theta$  of  $37.2^\circ$ ,  $43.2^\circ$ ,  $62.2^\circ$ ,  $73.4^\circ$ , and  $77.8^\circ$ , as well, with a lattice constant of  $4.177 \text{ \AA}$ . The face-centered cubic structure with respect to JCPDS number (00-047-1049) indicates the crystalline nature of the catalyst, is also supported by the diffraction peaks of nickel oxide nano particles. Nonetheless, the particle size is impacted by the peaks' broadening (Fardood *et al.* 2024), reported a face-centered cubic structure of a similar sort. The average size of the NiO nanoparticles was determined using Scherrer's method, and reported as 22 nm. The reported crystallite size (22 nm) and band gap (3.17 eV) suggest that the synthesized NiO nanoparticles are well-suited for photocatalytic applications (Moradnia *et al.* 2024), and the small particle size is beneficial for improving the catalytic activity.

### 3.3. FTIR analysis

Figure 2C shows the FTIR spectra of synthesized NiO nanoparticles, which show several significant absorption peaks. There were prominent peaks in  $3423$ ,  $2345$ ,  $1624$ ,  $1401$ ,  $665$ , and  $444 \text{ cm}^{-1}$ . The absorption band in the region of  $450\text{--}700 \text{ cm}^{-1}$  is assigned to Ni–O stretching vibration mode and the broadness of the absorption band indicates that the NiO nanoparticles are nanoparticles. The wide band at  $3423 \text{ cm}^{-1}$  and  $1624 \text{ cm}^{-1}$  shows the presence of O–H and N–H groups. The peaks at  $1401 \text{ cm}^{-1}$  are due to C–O stretching. Finally, the peak at  $444 \text{ cm}^{-1}$  which falls within the range of metal-oxide stretching vibration confirms the formation of NiO nanoparticles (Qiao *et al.* 2009).

### 3.4. Morphological characterization

The surface composition as well as morphology of synthesized NiO nanoparticles is shown in Figure 3. The SEM confirmation of the non-homogeneity and agglomeration among the particles is depicted in Figure 3A. EDAX confirmed the existence of NiO nanoparticles (Figure 3B). It was discovered that O and Ni had weight percentages of 23.17% and 76.83%, respectively. The size and shape of the NiO nanoparticles were assessed by TEM is shown in Figure 3C. The NiO nanoparticles are hexagonally aggregated and are non-homogeneous, as the TEM images demonstrate. The average particle size was within 10–25 nm. Inter planar spacing (d) had been determined with SAED patterns (Figure 3D). The lattice fringes of NiO nanoparticles are represented in Figure 3E. The distance that existed of the two bright areas was  $4.021 \text{ nm}$ , while the d-spacing was calculated to be  $0.23 \text{ nm}$ . It was an acceptable agreement with the crystalline diameters and the results of the XRD (Puttaswamy *et al.* 2018).

### 3.5. Adsorption–desorption analysis

For nickel oxide, the calculated surface area can be calculated with the nitrogen adsorption-desorption method. The resultant isotherm was found to be similar to type IV behavior (Figure 4A) and shows the characteristic pore dimensions of  $<2 \text{ nm}$ . The surface area of the synthesized nickel oxide nanoparticle was calculated to be  $2.56 \text{ m}^2/\text{g}$ . Effectively enhancing photocatalysis, the measured surface area of NiO nanoparticles is directly proportional to the accessible surface area. Figure 4B illustrates the pore size curve

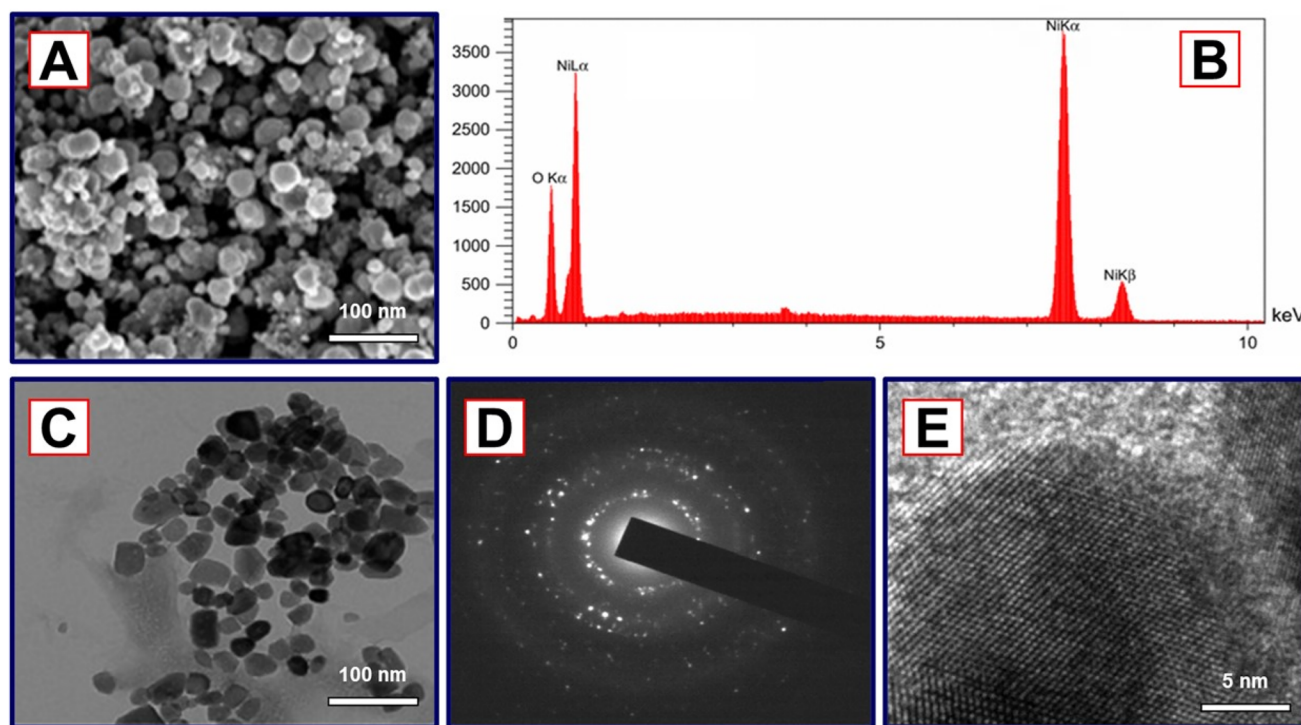


Figure 3. Synthesized NiO nanoparticles; (A) SEM, (B) EDAX spectrum, (C) TEM, (D) SAED pattern, and (E) lattice fringes.



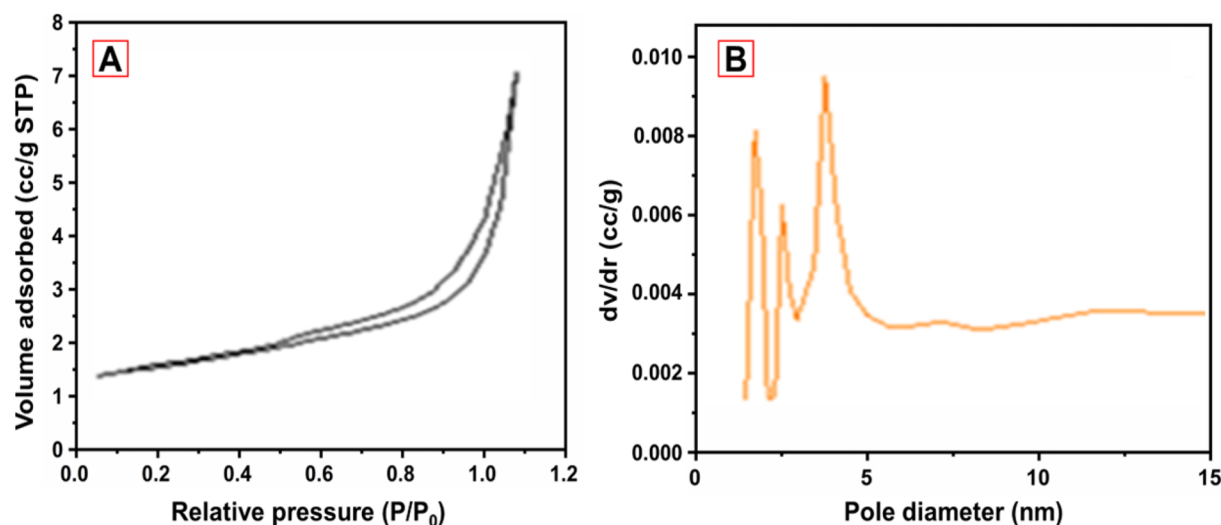


Figure 4. (A)  $N_2$  adsorption and desorption isotherm plot and (B) pore size distribution.

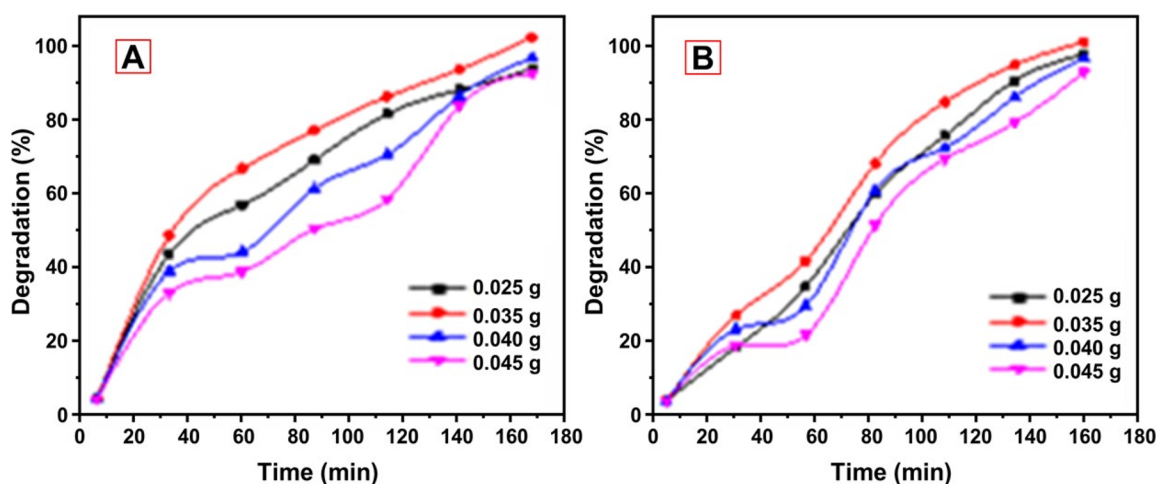


Figure 5. Effect of catalyst concentration (0.025–0.045 g) on (A) MG, and (B) JGB degradation.

distribution that has several peaks, indicating the existence of distinct pore size distributions within a 15 nm range. TEM confirmed the existence of distinct particle sizes. Within a range of 100 nm, the pore size distribution was discovered (Liu *et al.* 2025).

### 3.6. Dye degradation experimental procedure

50 mL of distilled water were mixed with 0.025 g of MG and 0.015 g of JGB dye to produce a stock solution. The 10 mL of dye from the stock solution were further diluted to 50 mL using double-distilled water for each experiment, and 0.01 N HCl was added to bring the pH decrease to 4. The whole system was set up on a magnetic stirrer and placed in to direct sunlight for 180 min. The average light intensity was estimated to be  $925 \times 100$  Lux. A 5 mL sample was collected at every 30 min during the experiment for use in a UV-visible spectrophotometer to observe the degradation process. A 100 mL was used for each batch experiment and side by side as a precautionary effect it has been closed by petri plates to avoid evaporation of the sample in direct sunlight (Al-Sehemi

*et al.* 2014; Zeng *et al.* 2016; Arunachalam *et al.* 2017; Santhosh *et al.* 2020). The equation was used to calculate the percentage of degradation.

$$D = \left( \frac{A_0 - A_t}{A_0} \right) \times 100 \quad (2)$$

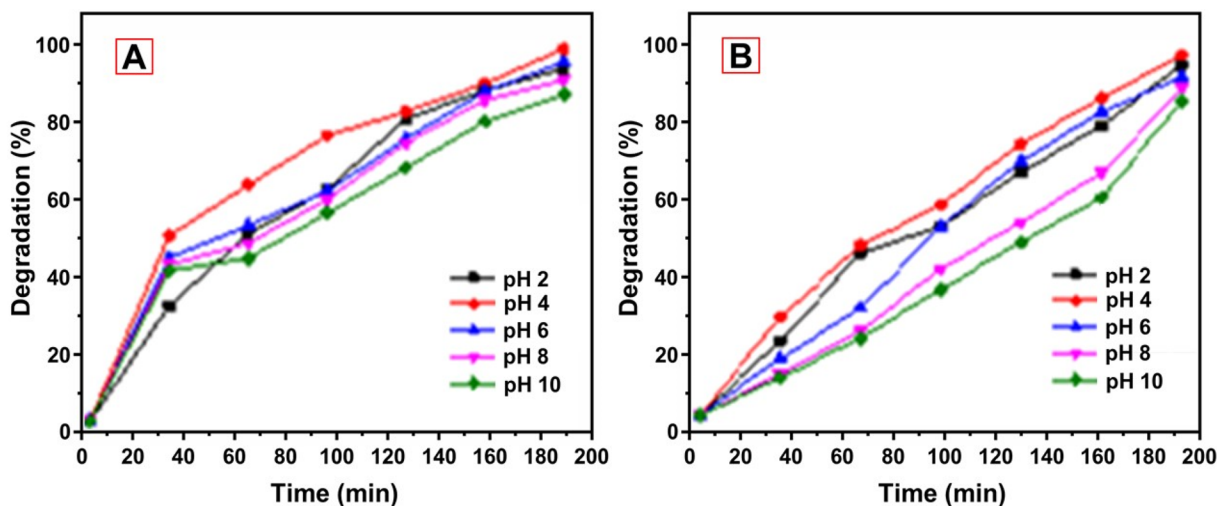
where;  $A_0$  is absorbance of the sample at the initial stage, and  $A_t$  is absorbance of the sample at time  $t$  (after 180 min).

#### 3.6.1. Influence of catalyst concentration

The effect of NiO nanoparticles loading on the removal of MG and JGB dye was investigated by increasing the catalyst concentration from 0.025 to 0.045 g with the dye concentration constant at pH 7 at  $1 \times 10^{-4}$  mol/dm<sup>3</sup> (Figure 5A,B). The degradation efficiency enhanced as the concentration of NiO nanoparticles increased due to the increased amount of dye that was adsorbed on the NiO nanoparticles surface (Table 1). The separation between the sample and the catalyst surface decreased the degradation with further increases in catalyst concentration. Agglomeration between the dye and NiO nanoparticles molecules lowers the amount of available

**Table 1.** Degradation percentage of the analyzed samples.

S. No	Catalyst concentration (g)	MG	JGB	pH	MG	JGB	Dye concentration (mol/dm <sup>3</sup> )	MG	JGB
		% degradation			% degradation			% degradation	
1.	0.025	88.12	92.06	2	91.89	93.50	$1 \times 10^{-4}$	97.10	96.07
2.	0.030	–	95.39	4	97.10	96.07	$2 \times 10^{-4}$	86.98	90.98
3.	0.035	96.63	91.03	6	93.65	90.23	$3 \times 10^{-4}$	80.00	87.55
4.	0.040	91.04	87.40	8	89.03	87.43	$4 \times 10^{-4}$	71.41	84.39

**Figure 6.** Influence of pH on (A) MG and (B) JGB samples.

and lessens light penetration through the solution (Babar *et al.* 2019; Dhanalakshmi *et al.* 2019; Honarmand *et al.* 2019; Saikumari *et al.* 2019). Our results regarding heterogeneous photo catalysts are well correlated with those reported by Santhosh *et al.* (2020). Therefore, the optimal load for the catalyst was found.

### 3.6.2. Effect of pH

The ideal pH range for degrading MG and JGB dyes was found by varying it between 2 and 10, while maintaining a constant catalyst loading of 0.035 and 0.030 g/50 mL, and  $1 \times 10^{-4}$  mol/dm<sup>3</sup> as strength of the sample dye. Table 1 and Figure 6 present degradation pattern of dye samples. For both dyes, extent of degradation increased for pH 2–4 and decreased for pH 10. For both dyes, the greatest degradation percentage was attained for pH 4. Previous studies have reported findings similar to these (Boruah *et al.* 2016; Santhosh *et al.* 2020). Our findings showed that the acidic medium had a higher rate of MG and JGB degradation. Photoelectrons convert a significant amount of O<sub>2</sub> into O<sub>2</sub><sup>•−</sup> radicals at acidic pH levels. The transfer of photoelectrons is facilitated by the positively charged surface of the photocatalyst. Due to the attractive electrostatic force between the dyes and the catalyst, a positive charge of the photo catalyst, the maximum amount of dye removal was achieved, increasing overall percentage of adsorption and degradation (Shilpa *et al.* 2020; Fu *et al.* 2025). Nonetheless, the dyes' degradation is aided by the production of OH<sup>−</sup> ions and their approach toward adsorption sites of the dye molecules on the NiO nanoparticles. The same factor as mentioned earlier reduces the degradation efficiency above the optimal pH

(>4). Moreover, the catalyst's amphoteric nature might be another factor contributing to the decline (Kale *et al.* 2019; Isai and Shrivastava 2019).

### 3.6.3. Effect of initial concentration of dye

The concentration of dye can be essential for the removal of dye samples from any solution. The concentration of MG and JGB dyes has been changed from  $1 \times 10^{-4}$  to  $4 \times 10^{-4}$  mol/dm<sup>3</sup>, while the catalyst loading has remained constant at pH 4 between 0.035 and 0.030 g/50 mL. The degradation % indicated major results (Table 1 and Figure 7). As the dye concentration grew, it also increased the photocatalytic degradation efficiency. If the concentration of a specific dye increased more, the catalyst's degrading activity decreased and the quantity of time required to complete the process increased. If concentrations increase to  $>2 \times 10^{-4}$  mol/dm<sup>3</sup>, it is discovered that a sizable portion of the sample dye compounds have been absorbed on the catalyst's surface, limiting the entry of sunlight. The reverse effect is observed at minimal concentrations.

The catalyst produces fewer OH and superoxide radicals as a result of constant surface area, which results in fewer active sites (Duraimurugan *et al.* 2019; Kakhki *et al.* 2019; Nasiri *et al.* 2019). The similar results have been observed with other colors (Shilpa *et al.* 2019). The concentration of dye plays a crucial role in the removal process of dyes from an aqueous solution. For MG and JGB dyes, the concentration was varied between  $1 \times 10^{-4}$  and  $4 \times 10^{-4}$  mol/dm<sup>3</sup> while maintaining the same catalyst amount varying from 0.035 to 0.030 g/50 mL at pH 4 experimentally. The percentage degradation results (as presented in Figure 7)

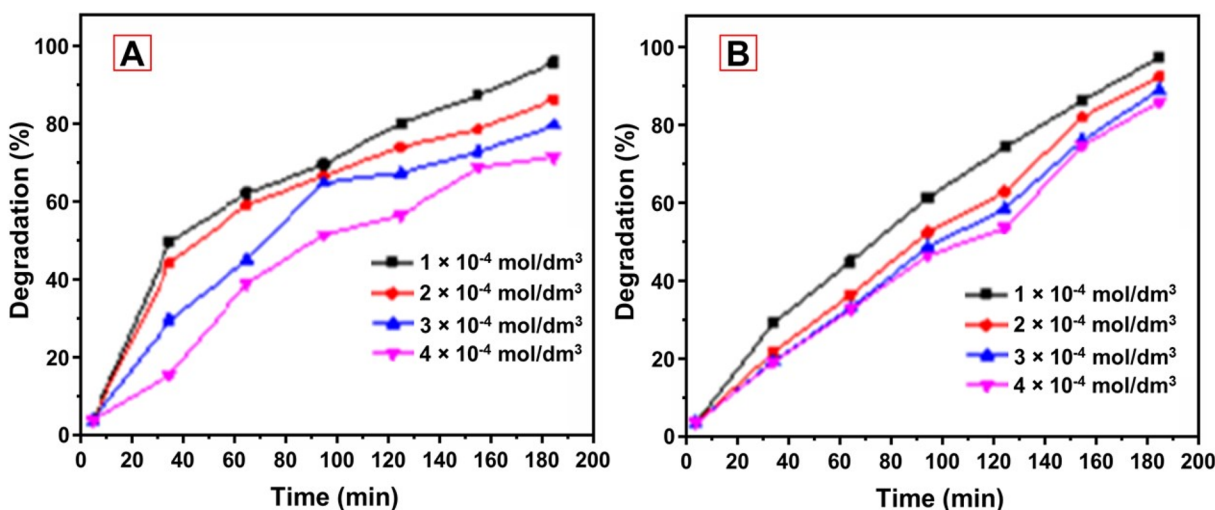


Figure 7. Influence of initial dye concentration on (A) MG and (B) JGB degradation.

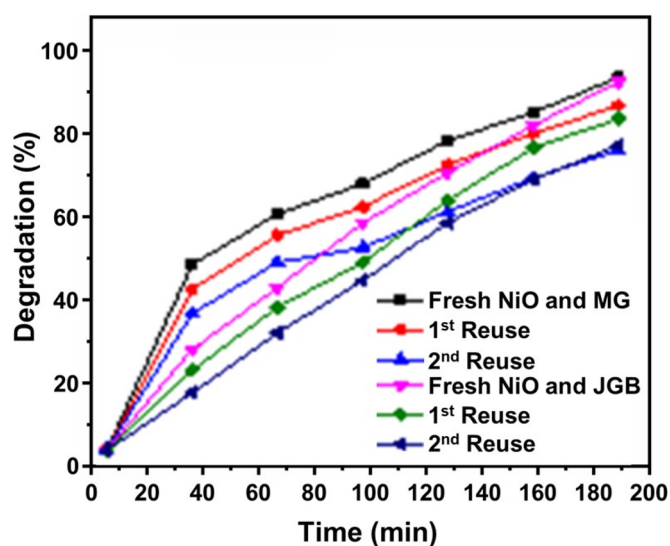


Figure 8. Reuse of catalyst.

showed notable trends. The photocatalytic degradation efficiency increased with dye concentrations up to  $1 \times 10^{-4}$  mol/dm<sup>3</sup>. However, at concentrations exceeding  $1 \times 10^{-4}$  mol/dm<sup>3</sup> the time taken for the whole degradation increased and thereby overall efficiency decreased. This decline in activity at higher concentration is attributed to the accumulation of a greater number of dye molecules onto the surface of the catalyst, which obstructs the light penetration into the solution. Conversely, at lower concentrations, the reduced availability of active sites due to the fixed surface area of the catalyst leads to saturation, resulting in decreased generation of superoxide and hydroxyl radicals. Similar trends have been observed with other dyes, as reported in the literature (Duraimurugan *et al.* 2019; Kakhki *et al.* 2019; Nasiri *et al.* 2019). The results showed a clear and efficient degradation of pollutants at an optimal pH (pH = 4), which suggests that the material is suitable for real-world applications under various conditions.

### 3.7. Reuse of catalyst

The synthesized NiO NPs' reusability was investigated, and the results demonstrated that during the consecutive cycles, the degradation efficiency for MG and JGB were 88.6% and 77.9%, respectively (Figure 8). The bleaching of the surface of the nanoparticles, reduced surface area, and a small quantity of catalyst loss while washing are the causes of the observed reduction in efficiency. With these limitations, the nanoparticles produced exhibited significant reusability and the potential for extensive water treatment applications (Santhosh, Yogendra, Madhusudhana *et al.* 2020; Santhosh, Yogendra, Mahadevan, *et al.* 2020). The study's limitations include a narrow scope of pollutants tested (only MG and JGB), lacking long-term stability and reusability testing of NiO nanoparticles. Additionally, there is limited investigation into the degradation mechanisms, environmental impact, and the influence of external variables like light intensity and temperature on photocatalytic performance. Finally, the study uses a single synthesis method, and advanced characterization techniques could provide more in-depth insights into the material's properties.

## 4. Conclusions

We used the SCM method to synthesize NiO nanoparticles. Analytical techniques verified the crystallite size, surface area, morphology and elemental composition and optical properties etc. and thus characterize the unique nature of synthesized nanoparticles. The crystallite size and  $E_g$  (band gap) of the cubic-structure catalyst were determined as 22 nm and 3.17 eV. TEM confirmed that the particle size was less than 25 nm. The study inspected the efficacy of MG and JGB as pollutants in water, finding that both dyes degraded to their maximum extent at pH = 4. Furthermore, the NiO nanoparticles that was utilized to treat wastewater contaminated with MG and JGB showed increased photocatalytic activity in a quicker and more economical manner. In future this work can contribute to the development of more efficient, stable, and scalable NiO nanoparticles as a promising



photocatalyst for wastewater treatment and environmental remediation.

## Acknowledgments

The authors acknowledge and appreciate the Ongoing Research Funding Program (ORF-2025-774), King Saud University, Riyadh, Saudi Arabia. This work was supported by the “2024 System Semiconductor Technology Development Program” funded by the Chungbuk Technopark.

## Ethical approval

This manuscript did not involve any human participants, human data, human tissues, or cloned animals hence ethical approval is not applicable.

## Disclosure statement

No potential conflict of interest was reported by the authors.

## Consent to publish

All authors have full consent to publish the content of the manuscript.

## Data availability statement

The data that support the findings of this study are available from the corresponding author upon reasonable request.

## ORCID

Raja Venkatesan  <http://orcid.org/0000-0002-5547-7477>

## References

- Abd-El-Lateef HM, Khalaf MM, Al-Omair MA, Dao VD, Mohamed IMA. 2020. Chemical synthesis of NiO nanostructure by surfactant-assisted sol-gel methodology for urea electrocatalytic oxidation. *Mater Lett.* 276:128192. doi: [10.1016/j.matlet.2020.128192](https://doi.org/10.1016/j.matlet.2020.128192).
- Ahamed ST, Bhar SK, Mondal A. 2019. Formation of a TiO<sub>2</sub>/CdS/Pd heterojunction and study of their photocatalytic degradation of organic dyes and toxic metal ion reduction. *J Mater Sci: Mater Electron.* 30(5):4400–4408. doi: [10.1007/s10854-019-00729-y](https://doi.org/10.1007/s10854-019-00729-y).
- Ahmad W, Bhatt SC, Verma M, Kumar V, Kim H. 2022. A review on current trends in the green synthesis of nickel oxide nano particles, characterizations, and their applications. *Environ Nanotechnol Mon Manage.* 18:100674. doi: [10.1016/j.enmm.2022.100674](https://doi.org/10.1016/j.enmm.2022.100674).
- Al-Musawi TJ, Rajiv P, Mengelizadeh N, Mohammed IA, Balarak D. 2021. Development of sono photocatalytic process for degradation of acid orange 7 dye by using titanium dioxide nanoparticles/graphene oxide nanocomposite as a catalyst. *J Environ Manag.* 292:112777. doi: [10.1016/j.JEM.2021.112777](https://doi.org/10.1016/j.JEM.2021.112777).
- Al-Sehemi AG, Al-Shihri AS, Kalam A, Du G, Ahmad T. 2014. Microwave synthesis, optical properties and surface area studies of NiO nano particles. *J Mol Struct.* 1058:56–61. doi: [10.1016/j.mol-struct.2013.10.065](https://doi.org/10.1016/j.mol-struct.2013.10.065).
- Arunachalam P, Ghanem MA, Al-Mayouf AM, Al-Shalwi M, Abd-Elkader OH. 2017. Microwave assisted synthesis and characterization of Ni/NiO nano particles as electrocatalyst for methanol oxidation in alkaline solution. *Mater Res Express.* 4(2):025035. doi: [10.1088/2053-1591/aa5ed8](https://doi.org/10.1088/2053-1591/aa5ed8).
- Balarak D, Al Musawi TJ, Mohammed IA, Abasizadeh H. 2020. The eradication of reactive black 5 dye liquid wastes using *Azolla filiculoides* aquatic fern as a good and an economical biosorption agent. *SN Appl Sci.* 2(6):1015. - doi: [10.1007/s42452-020-2841-x](https://doi.org/10.1007/s42452-020-2841-x).
- Balarak D, Zafariyan M, Igwegbe CA, Onyechi KK, Ighalo JO. 2021. Adsorption of acid blue 92 dye from aqueous solutions by single-walled carbon nanotubes: isothermal, kinetic, and thermodynamic studies. *Environ Process.* 8(2):869–888. doi: [10.1007/s40710-021-00505-3](https://doi.org/10.1007/s40710-021-00505-3).
- Balarak D, Abasizadeh HA, Yang J-K, Shim MJ, Lee S-M. 2020. Biosorption of acid orange 7 (AO7) dye by canola waste: equilibrium, kinetic and thermodynamics studies. *Desalin Water Treat.* 190:331–339. doi: [10.5004/dwt.2020.25665](https://doi.org/10.5004/dwt.2020.25665).
- Bomila R, Suresh S, Srinivasan S. 2019. Synthesis, characterization and comparative studies of dual doped ZnO nano particles for photocatalytic applications. *J Mater Sci: Mater Electron.* 30(1):582–592. doi: [10.1007/s10854-018-0324-2](https://doi.org/10.1007/s10854-018-0324-2).
- Boruah PK, Borthakur P, Darabdhara G, Kamaja CK, Karbhal I, Shelke MV, Phukan P, Saikia D, Das MR. 2016. Sunlight assisted degradation of dye molecules and reduction of toxic Cr (VI) in aqueous medium using magnetically recoverable Fe<sub>3</sub>O<sub>4</sub>/reduced graphene oxide nanocomposite. *RSC Adv.* 6(13):11049–11063. doi: [10.1039/C5RA25035H](https://doi.org/10.1039/C5RA25035H).
- Chaudhary GR, Saharan P, Umar A, Mehta SK, Mor S. 2013. Well-crystalline ZnO nanostructures for the removal of acridine orange and coomassie brilliant blue R-250 hazardous dyes. *Sci Adv Mat.* 5(12):1886–1894. doi: [10.1166/sam.2013.1701](https://doi.org/10.1166/sam.2013.1701).
- Dhanalakshmi S, Kumar PS, Karuthapandian S, Muthuraj V, Prithivikumar V. 2019. Design of Gd<sub>2</sub>O<sub>3</sub> nanorods: a challenging photo catalyst for the degradation of neurotoxicity chloramphenicol drug. *J Mater Sci: Mater Electron.* 30(4):3744–3752. doi: [10.1007/s10854-018-00656-4](https://doi.org/10.1007/s10854-018-00656-4).
- Duraimurugan J, Kumar SG, Maadeswaran P, Shanavas S, Anbarasan PM, Vasudevan V. 2019. Structural, optical and photocatalytic properties of zinc oxide nano particles obtained by simple plant extract mediated synthesis. *J Mater Sci: Mater Electron.* 30(2):1927–1935. doi: [10.1007/s10854-018-0466-2](https://doi.org/10.1007/s10854-018-0466-2).
- Ebin B. 2018. Simple preparation of Ni and NiO nano particles using raffinate solution originated from spent NiMH battery recycling. *J Inorg Organomet Polym.* 28(6):2554–2563. doi: [10.1007/s10904-018-0926-4](https://doi.org/10.1007/s10904-018-0926-4).
- Faraji AR, Farahani AR, Khoramdareh NB, Gil S, Jafari A, Hekmatian N, Shojaei Z. 2023. Cu-Fe nanoparticles decorated rice hull/chitosan@FeAl<sub>2</sub>O<sub>4</sub> to boosted peroxidase-like activity for catalytic degradation of antibiotics: kinetics and mechanistic insights. *J Environ Chem Eng.* 11(6):111348. doi: [10.1016/j.jece.2023.111348](https://doi.org/10.1016/j.jece.2023.111348).
- Faraji AR, Khoramdareh NB, Falahati F, Jafari S, Monfared SA, Faghhi A. 2023. Superparamagnetic Mn-Fe alloy composite derived from cross-binder of chitosan/rice husk waste/iron aluminate spinel hercynite for rapid catalytic detoxification of aflatoxin B1: structure, performance and synergistic mechanism. *Int J Biol Macromol.* 234:123709. doi: [10.1016/j.ijbiomac.2023.123709](https://doi.org/10.1016/j.ijbiomac.2023.123709).
- Fardood ST, Ganjkanlu S, Moradnia F, Ramazani A. 2024. Green synthesis, characterization, and photocatalytic activity of super paramagnetic MgFe<sub>2</sub>O<sub>4</sub>@ZnAl<sub>2</sub>O<sub>4</sub> nanocomposites. *Sci Rep.* 14(1):16670. doi: [10.1038/s41598-024-67655-w](https://doi.org/10.1038/s41598-024-67655-w).
- Fardood ST, Moradnia F, Aminabhavi TM. 2024. Green synthesis of novel Zn<sub>0.5</sub>Ni<sub>0.5</sub>FeCrO<sub>4</sub> spinel magnetic nanoparticles: photodegradation of 4-nitrophenol and aniline under visible light irradiation. *Environ Pollut.* 358:124534. doi: [10.1016/j.envpol.2024.124534](https://doi.org/10.1016/j.envpol.2024.124534).
- Fardood ST, Moradnia F, Zare FY, Heidarzadeh S, Majedi MA, Ramazani A, Sillanpää M, Nguyen K. 2024. Green synthesis and characterization of αMn<sub>2</sub>O<sub>3</sub> nanoparticles for antibacterial activity and efficient visible-light photocatalysis. *Sci. Rep.* 14:6755. doi: [10.1038/s41598-024-56666-2](https://doi.org/10.1038/s41598-024-56666-2).
- Fardood ST, Moradnia F, Ganjkanlu S, Ouni L, Ramazani A, Sillanpää M. 2024. Green synthesis and characterization of spinel CoAl<sub>2</sub>O<sub>4</sub> nanoparticles: efficient photocatalytic degradation of organic dyes. *Inorg Chem Comm.* 167:112719. doi: [10.1016/j.inoche.2024.112719](https://doi.org/10.1016/j.inoche.2024.112719).

- Fu L, Wang J, Fu X, Zhao G. 2025. Finite-time Pade-based adaptive FNN controller implementation for microbial fuel cell with delay and multi-disturbance. *Int J Hydrogen Energy*. 98:1034–1043. doi: [10.1016/j.ijhydene.2024.10.372](https://doi.org/10.1016/j.ijhydene.2024.10.372).
- Hassan HB, Hashim A, Abduljalil HM. 2023. Synthesis, structural and optical characteristics of PEO/NiO/In<sub>2</sub>O<sub>3</sub> hybrid nanomaterials for photodegradation of pollutants from wastewater. *Opt Quant Electron*. 55(6):556. doi: [10.1007/s11082-023-04830-9](https://doi.org/10.1007/s11082-023-04830-9).
- Honarmand MM, Mehr ME, Yarahmadi M, Siadat MH. 2019. Effects of different surfactants on morphology of TiO<sub>2</sub> and Zr-doped TiO<sub>2</sub> nano particles and their applications in MB dye photocatalytic degradation. *SN Appl Sci*. 1(5):505. doi: [10.1007/s42452-019-0522-4](https://doi.org/10.1007/s42452-019-0522-4).
- Isai KP, Shrivastava VS. 2019. Photocatalytic degradation of methylene blue using ZnO and 2%Fe-ZnO semiconductor nanomaterials synthesized by sol-gel method: a comparative study. *SN Appl Sci*. 1(10):1247. doi: [10.1007/s42452-019-1279-5](https://doi.org/10.1007/s42452-019-1279-5).
- Jamal A, Rahman MM, Faisal M, Khan SB. 2011. Studies on photocatalytic degradation of acridine orange and chloroform sensing using as-grown antimony oxide microstructures. *MSA*. 2(6):676–683. doi: [10.4236/msa.2011.26093](https://doi.org/10.4236/msa.2011.26093).
- Jamil YMS, Awad MAH, Al-Maydama HMA, EL-Ghoul Y, Al-Hakimi AN. 2022. Synthesis and study of enhanced electrochemical properties of NiO nanoparticles deposited on TiO<sub>2</sub> nanotubes. *Appl Organom Chemis*. 36(9):e6795. doi: [10.1002/aoc.6795](https://doi.org/10.1002/aoc.6795).
- Jiang L, Du G-C, Wang J-P, Wu Z-X, Li H-Y. 2025. Eco-friendly efficient separation of Cr(VI) from industrial sodium vanadate leaching liquor for resource valorization. *Sep Purif Technol*. 361:131673. doi: [10.1016/j.seppur.2025.131673](https://doi.org/10.1016/j.seppur.2025.131673).
- Kakhki RM, Hedayat S, Mohammadzadeh K. 2019. Novel, green and low-cost synthesis of Ag nanoparticles with superior adsorption and solar based photocatalytic activity. *J Mater Sci: Mater Electron*. 30(9):8788–8795. doi: [10.1007/s10854-019-01203-5](https://doi.org/10.1007/s10854-019-01203-5).
- Kale G, Arbuj S, Kawade U, Kadam S, Nikam L, Kale B. 2019. Paper templated synthesis of nanostructured Cu-ZnO and its enhanced photocatalytic activity under sunlight. *J Mater Sci: Mater Electron*. 30(7):7031–7042. doi: [10.1007/s10854-019-01020-w](https://doi.org/10.1007/s10854-019-01020-w).
- Kumar PV, Ahamed AJ, Karthikeyan M. 2019. Synthesis and characterization of NiO nano particles by chemical as well as green routes and their comparisons with respect to cytotoxic effect and toxicity studies in microbial and MCF-7 cancer cell models. *SN Appl Sci*. 1(9):1083. doi: [10.1007/s42452-019-1113-0](https://doi.org/10.1007/s42452-019-1113-0).
- Lin J, Cheng Q, Kumar A, Zhang W, Yu Z, Hui D, Zhang C, Shan S. 2025. Effect of degradable microplastics, biochar and their coexistence on soil organic matter decomposition: a critical review. *TrAC Trends Anal Chem*. 183:118082. doi: [10.1016/j.trac.2024.118082](https://doi.org/10.1016/j.trac.2024.118082).
- Liu S, Ndago AM, Chen B, Han S, Chen W, Zhang J, Zheng X. 2025. The influence of metal organic frameworks(MOFs) after tannic acid etching on the performance and structure of loose nanofiltration membranes for enhanced dyes/salts selective separation. *J Water Proc Eng*. 70:107009. doi: [10.1016/j.jwpe.2025.107009](https://doi.org/10.1016/j.jwpe.2025.107009).
- Mansour NB, Mir LE. 2017. Influence of the nickel oxide nanoparticles content on the electrical properties of carbon/nickel nanocomposites. *J Mater Sci: Mater Electron*. 28(15):11284–11291. doi: [10.1007/s10854-017-6919-1](https://doi.org/10.1007/s10854-017-6919-1).
- Moradnia F, Fardood ST, Zarei A, Heidarzadeh S, Ramazani A, Sillanpaa M. 2024. Green synthesis of nickel oxide nanoparticles using plant extracts: an overview of their antibacterial, catalytic, and photocatalytic efficiency in the degradation of organic pollutants. *Iran J Catal*. 14:1. doi: [10.57647/j.ijc.2024.1401.01](https://doi.org/10.57647/j.ijc.2024.1401.01).
- Nasiri A, Tamaddon F, Mosslemin MH, Gharaghani MA, Asadipour A. 2019. New magnetic nanobiocomposite CoFe<sub>2</sub>O<sub>4</sub>@methylcellulose: facile synthesis, characterization, and photocatalytic degradation of metronidazole. *J Mater Sci: Mater Electron*. 30(9):8595–8610. doi: [10.1007/s10854-019-01182-7](https://doi.org/10.1007/s10854-019-01182-7).
- Puttaswamy R, Suresh GS, Mahadevan KM, Nayak YA. 2018. Carbon-nanotube-encapsulated LiTiPO<sub>4</sub> composite electrode for aqueous rechargeable battery applications. *ChemistrySelect*. 3(11):3056–3069. doi: [10.1002/slct.201702132](https://doi.org/10.1002/slct.201702132).
- Qiao H, Wei Z, Yang H, Zhu L, Yan X. 2009. Preparation and characterization of NiO nanoparticles by anodic arc plasma method. *J Nanomater*. 2009(1):1–5. doi: [10.1155/2009/795928](https://doi.org/10.1155/2009/795928).
- Rao M, Xia H, Xu Y, Jiang G, Zhang Q, Yuan Y, Zhang L. 2024. Study on ultrasonic assisted intensive leaching of germanium from germanium concentrate using HCl/NaOCl. *Hydrometallurgy*. 230:106385. doi: [10.1016/j.hydromet.2024.106385](https://doi.org/10.1016/j.hydromet.2024.106385).
- Saffarzadeh S, Nabiyouni G, Heidary FA. 2019. Short time microwave method for synthesis of magnetic NiFe<sub>2</sub>O<sub>4</sub>/NiO nanocomposites as a clean technology in photocatalytic degradation of water pollutants. *J Mater Sci: Mater Electron*. 30(9):8171–8181. doi: [10.1007/s10854-019-01132-3](https://doi.org/10.1007/s10854-019-01132-3).
- Saikumari N, Preethi T, Abarna B, Rajarajeswari GR. 2019. Ecofriendly, green tea extract directed sol-gel synthesis of nano titania for photocatalytic application. *J Mater Sci: Mater Electron*. 30(7):6820–6831. doi: [10.1007/s10854-019-00994-x](https://doi.org/10.1007/s10854-019-00994-x).
- Salim E, Tarabiah AE. 2023. The Influence of NiO nanoparticles on structural, optical and dielectric properties of CMC/PVA/PEDOT: PSS nanocomposites. *J Inorg Organomet Polym*. 33(6):1638–1645. doi: [10.1007/s10904-023-02591-2](https://doi.org/10.1007/s10904-023-02591-2).
- Santhosh AM, Yogendra K, Madhusudhana N, Mahadevan KM, Mallikarjuna IH. 2020. Photocatalytic degradation of victoria blue B a cationic dye by synthesized zinc oxide nanoparticle. *IJNP*. 12(4):327–341. doi: [10.1504/IJNP.2020.112403](https://doi.org/10.1504/IJNP.2020.112403).
- Santhosh AM, Yogendra K, Mahadevan KM, Madhusudhana N. 2020. Application of synthesized tetragonal structured zirconium oxide nano particle on victoria blue B and acridine orange dye. *J Phys: Conf Ser*. 1495(1):012007. doi: [10.1088/1742-6596/1495/1/012007](https://doi.org/10.1088/1742-6596/1495/1/012007).
- Shilpa G, Yogendra K, Mahadevan KM, Madhusudhana N, Santhosh AM. 2020. Photodegradation of acid red 88 and direct green dyes using prepared nickel oxide nanoparticles. *Indian J Environ Prot*. 40:1192–1197.
- Shilpa G, Yogendra K, Mahadevan KM, Santhosh AM. 2019. Photocatalytic degradation of mono azo dye acid red 88 by using synthesized calcium aluminate nanoparticle and its kinetics. *Res J Chem Environ*. 23(10):29–35.
- Sivagami M, Asharani IV. 2022. Phyto-mediated Ni/NiO NPs and their catalytic applications-a shortreview. *Inorg Chem Commun*. 145:110054. doi: [10.1016/j.inoche.2022.110054](https://doi.org/10.1016/j.inoche.2022.110054).
- Taghizadeh MT, Kheljan FN, Vatanparast M. 2018. Ultrasonic-assisted synthesis of ZnO/NiO nanocomposites and kinetic study of their photocatalytic activity. *J Mater Sci: Mater Electron*. 29(2):978–984. doi: [10.1007/s10854-017-7995-y](https://doi.org/10.1007/s10854-017-7995-y).
- Yadav M, Ali S, Yadav OP. 2014. Photo-catalytic degradation of victoria blue-B dye using ZnS and Ag-N co-doped ZnS nanoparticles under visible radiation. *J Appl Chem*. 3:2563–2572.
- Zeng G, Li W, Ci S, Jia J, Wen Z. 2016. Highly dispersed NiO nanoparticles decorating graphene nanosheets for non-enzymatic glucose sensor and biofuel cell. *Sci Rep*. 6(1):36454. doi: [10.1038/srep36454](https://doi.org/10.1038/srep36454).
- Zhu Y, Dai H, Yuan S. 2023. The competition between heterotrophic denitrification and DNRA pathways in hyporheic zone and its impact on the fate of nitrate. *J. Hydrol*. 626:130175. doi: [10.1016/j.jhydrol.2023.130175](https://doi.org/10.1016/j.jhydrol.2023.130175).